# High-Precision X-ray Total Scattering Measurements using a High-Accuracy Detector System

Kenichi Kato

*RIKEN SPring-8 Center, Japan*

katok@spring8.or.jp

# Acknowledgements

Mr. K. Shigeta (*Nichigi*)
Mr. M. Fujita (*RSC*)
Ms. M. Yamamoto (*RSC*)

Prof. B. B. Iversen (*Aarhus Univ.*)
Prof. M. Yamauchi (*Kyushu Univ.*)
Prof. Y. Tanaka (*Univ. of Hyogo*)
Dr. T. Hatsui (*RSC*)

JST, PRESTO (Supervisor: Prof. Y. Amemiya)

# Precision & Accuracy of Observations

Accuracy: Bias from the true value = Systematic error

Precision: Deviation from the mean value = Random error

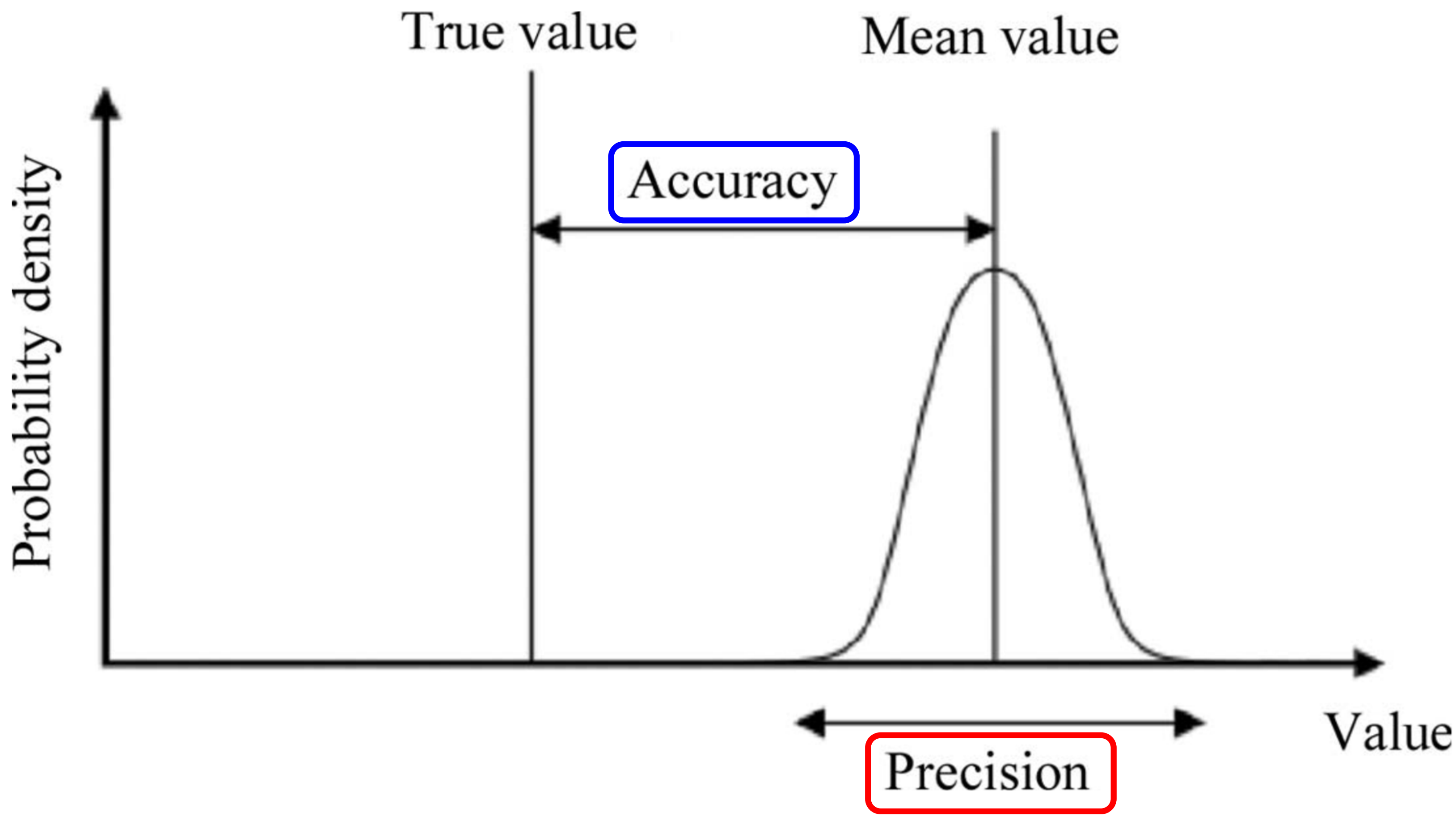


J. Helliwell, *Acta Cryst.* A77, 173 (**2021**).

# X-ray Total Scattering

**Ordered**

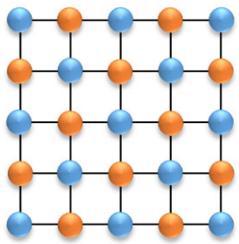

**Disordered**

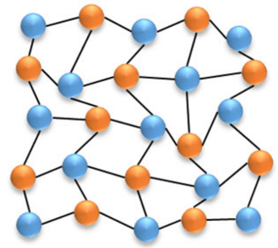

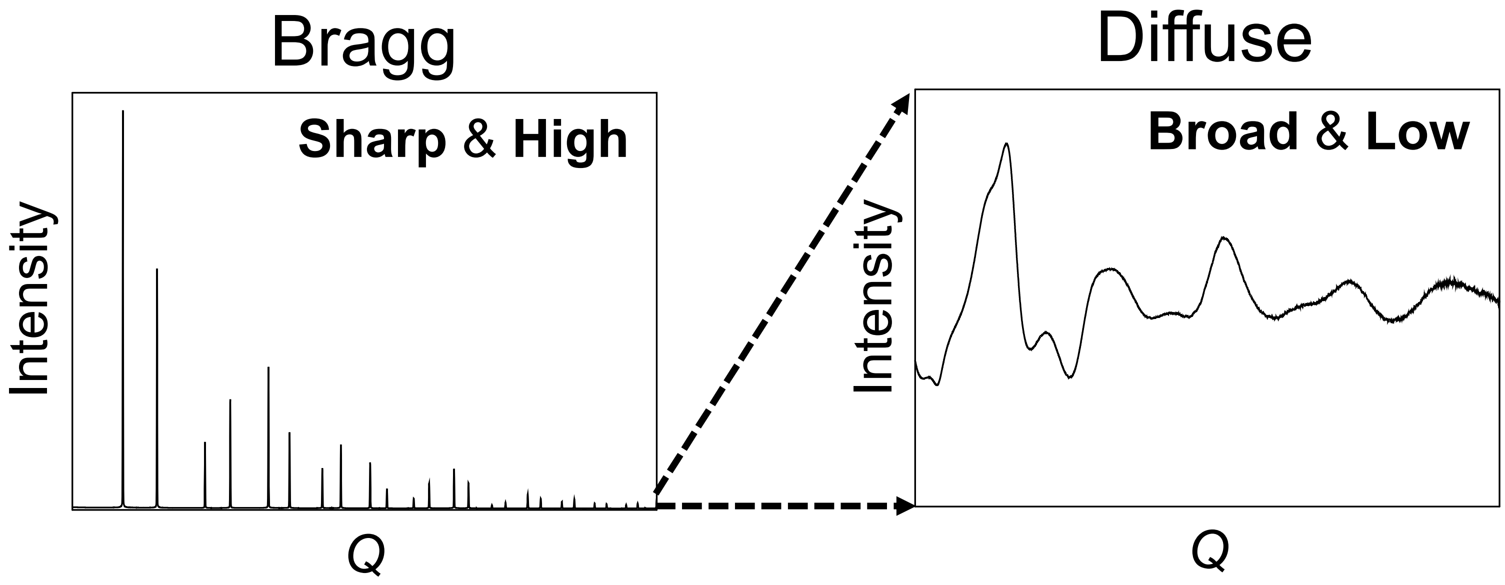


Scattering vector:
$Q = 4\pi \sin\theta / \lambda$

| | Required | Typical* |
|---|---|---|
| Q range (Å$^{-1}$) | ~30 | ~40 |
| Q step (Å$^{-1}$) | $10^{-3}$ | $10^{-2}$ |
| Precision | 0.1% | ? |

Trade-off

*P. J. Chupas et al., *J. Appl. Cyst.* 40, 463 (**2007**).

# Module Assembly for Total Scattering

K. Kato et al., *J. Synchrotron Rad.* 26, 762 (**2019**).

## **OHGI**: **O**verlapped **H**igh-**G**rade **I**ntelligencer

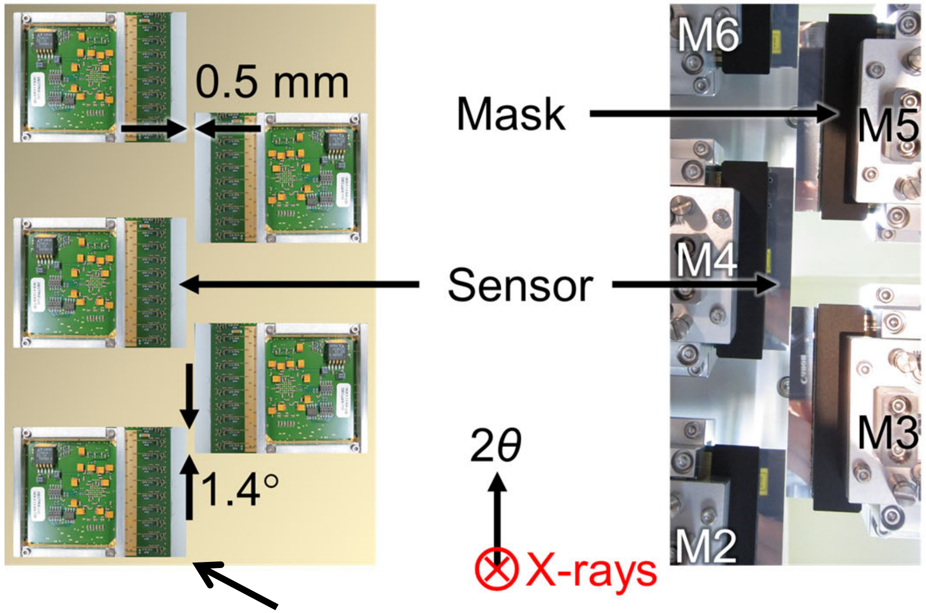


Si microstrip module
*MYTHEN by DECTRIS*

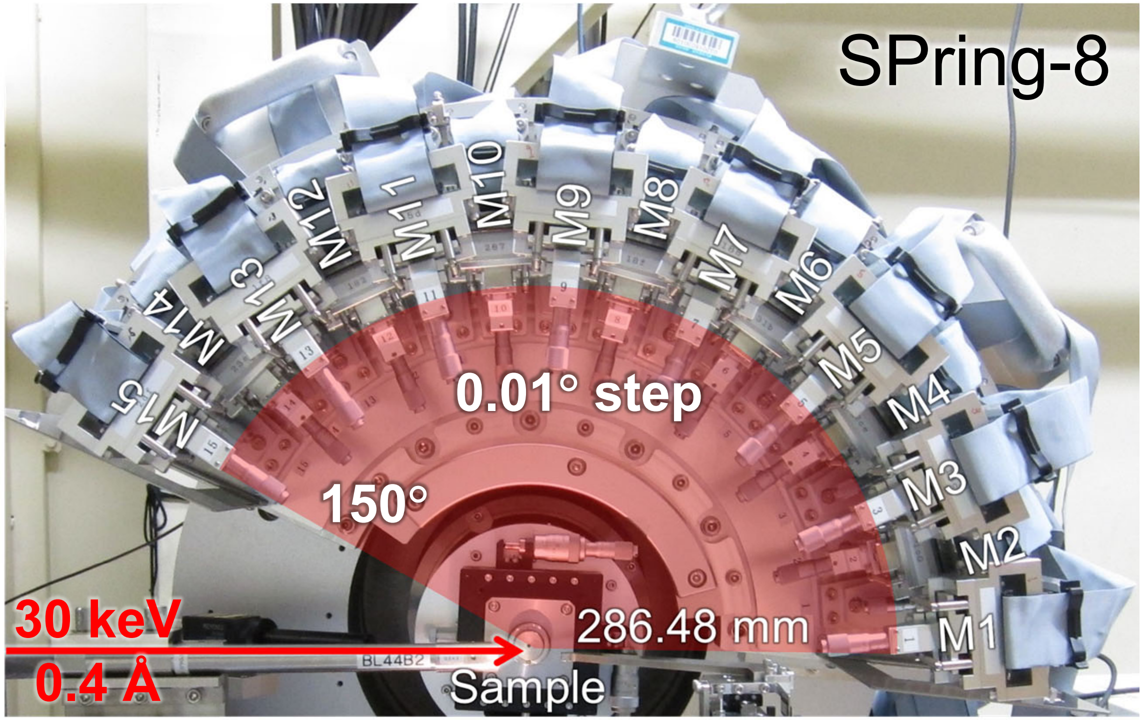


| | Required | OHGI |
|---|---|---|
| Q range (Å$^{-1}$) | ~30 | ~30 |
| Q step (Å$^{-1}$) | $10^{-3}$ | $10^{-3}$ |
| Precision | 0.1% | 1% |

$$Q = 4\pi \sin\theta / \lambda$$

# Precision reduced by Accuracy

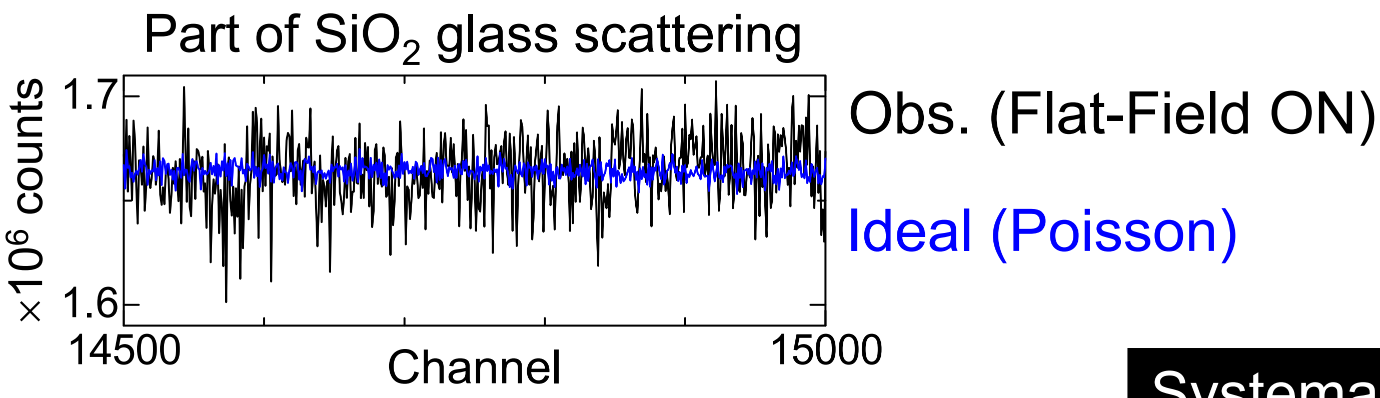


Systematic error or Inaccuracy: Differences in X-ray response between channels

Precision: $\frac{\sigma_I}{\bar{I}}$

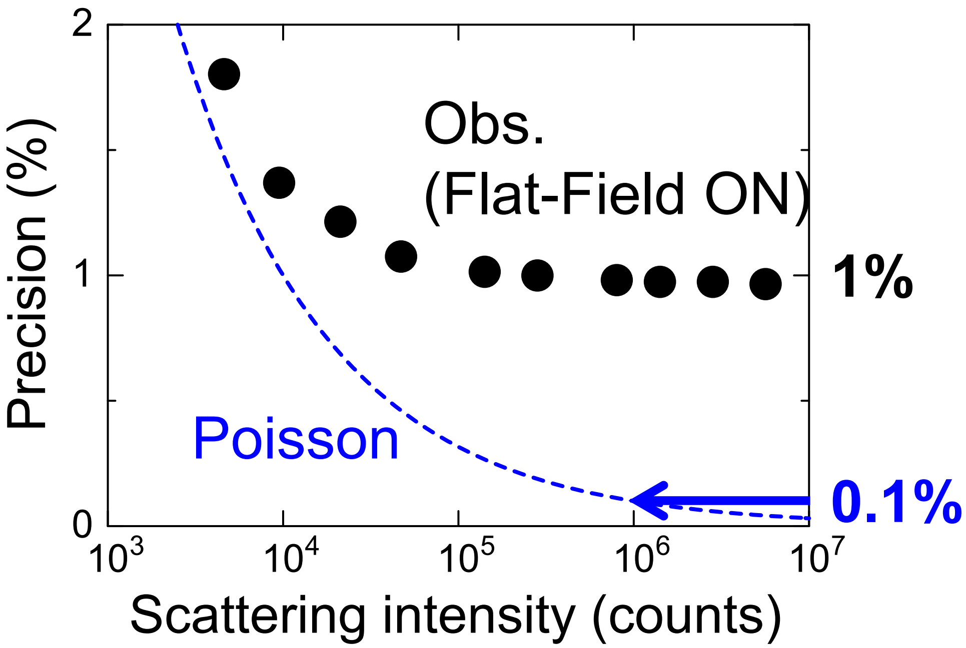

# Can we improve data precision?

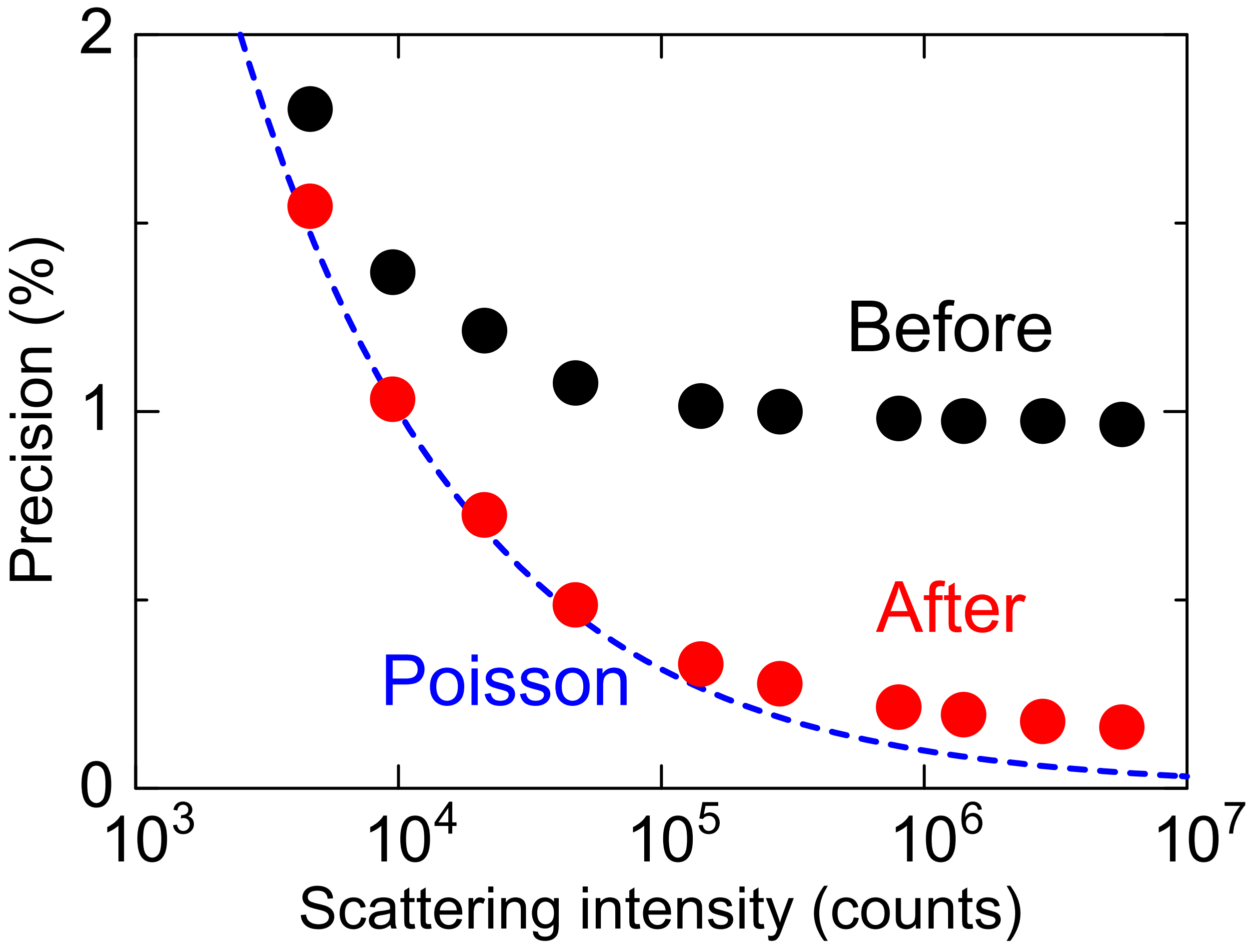

# Statistical Approach to Reference Intensity

Conventional (Flat-field):
Linear fitting to uniform reference intensity

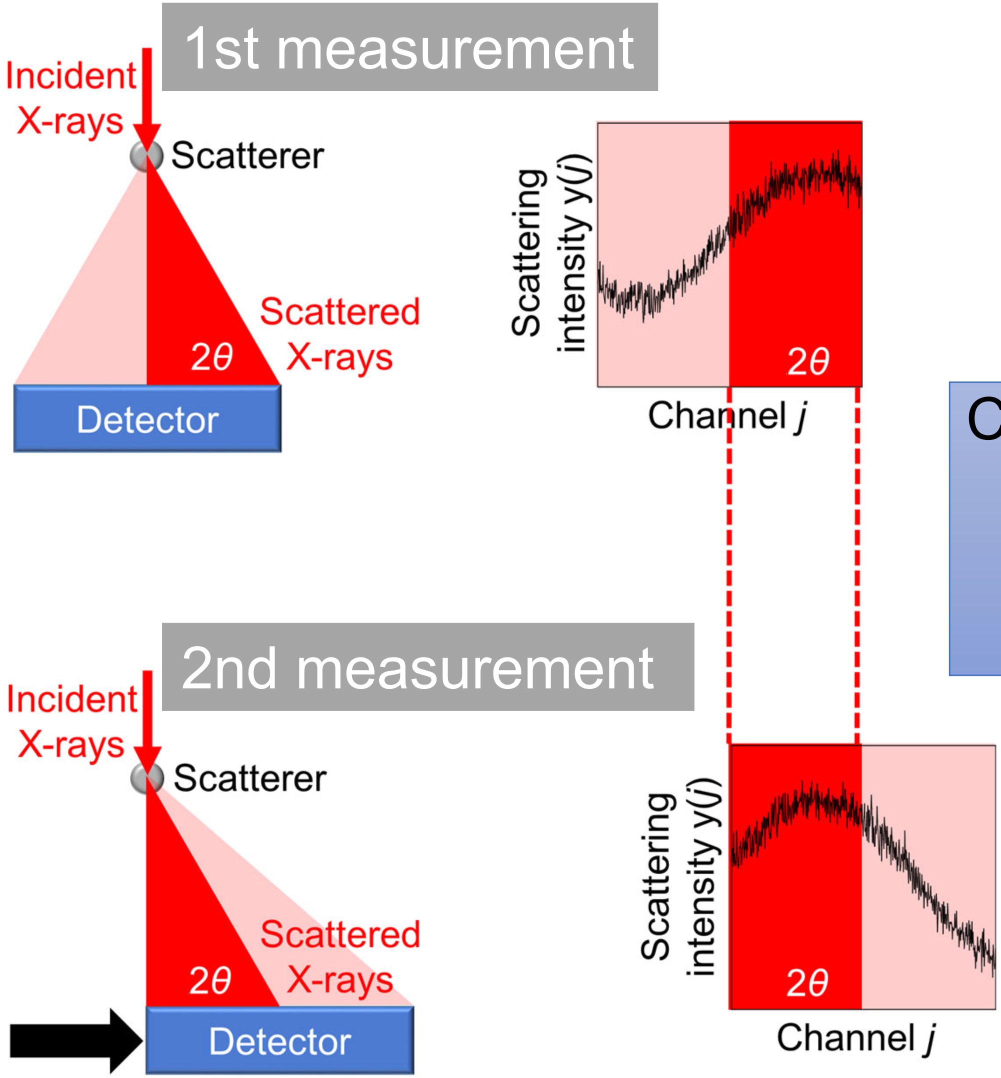


Correction factor for channel $j$

$$c(j) = \boxed{\frac{y_{2\theta}(j) + y_{2\theta}(j+\delta j)}{2}} \times \frac{1}{y_{2\theta}(j)}$$

Statistically estimated intensity at $2\theta$

# Time-Efficiency Problem

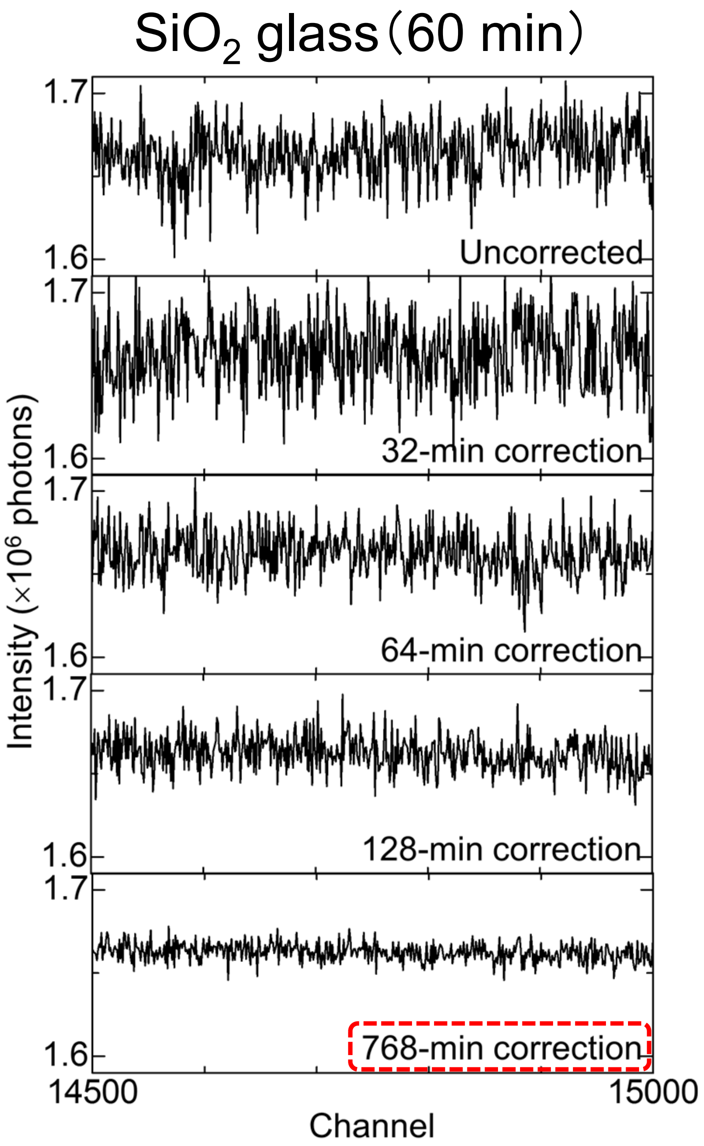


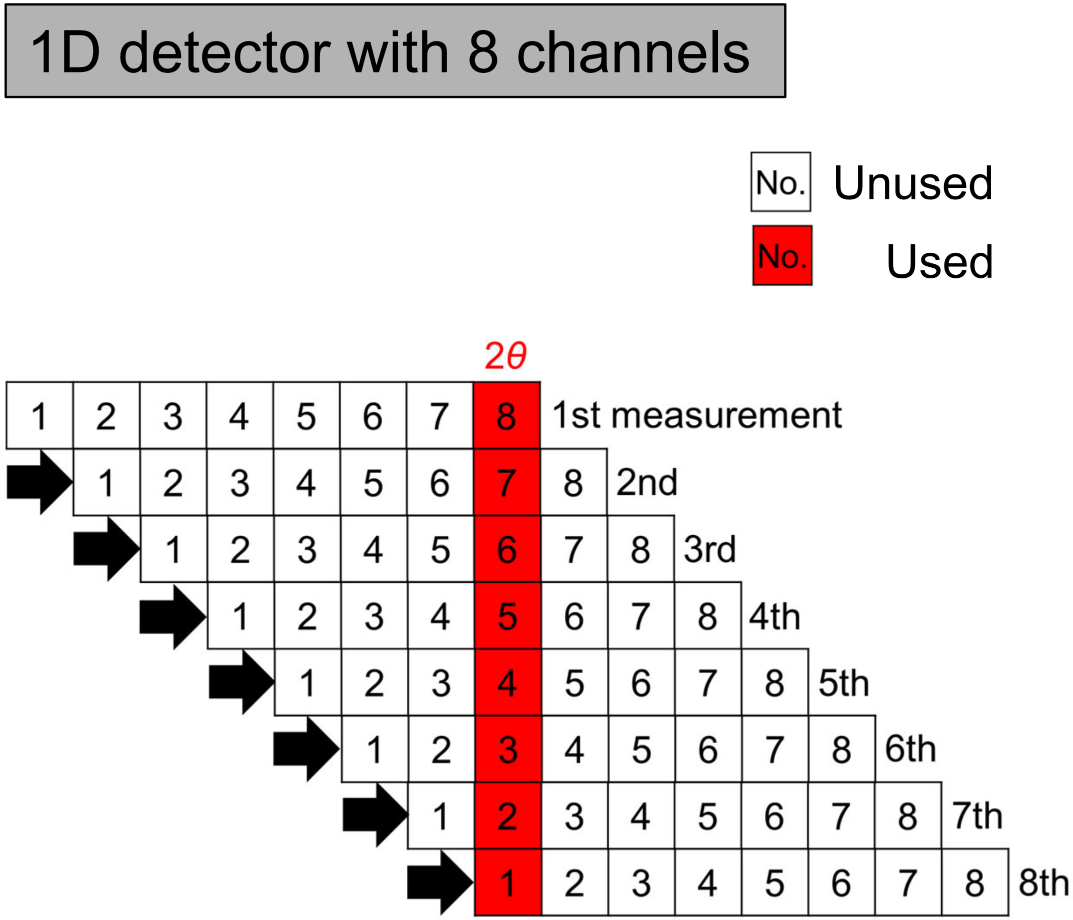

# Data-Driven Approach

K. Kato et al., *J. Synchrotron Rad.* 27, 1172 (**2020**).

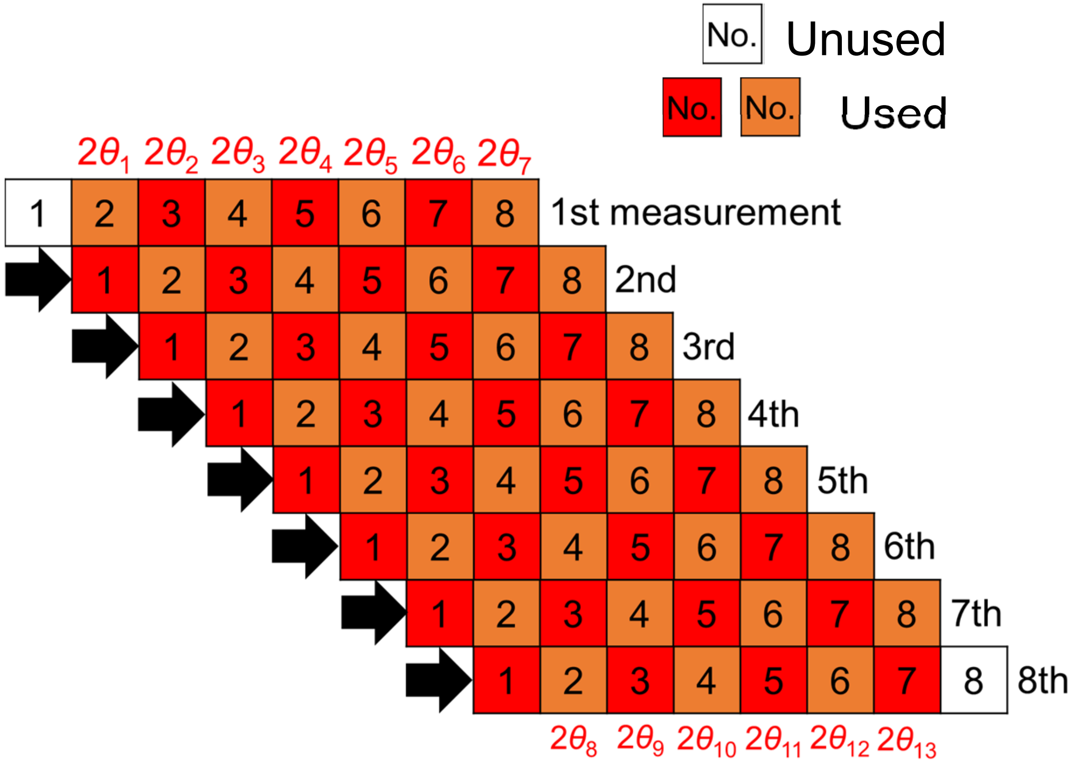


1D detector with 8 channels

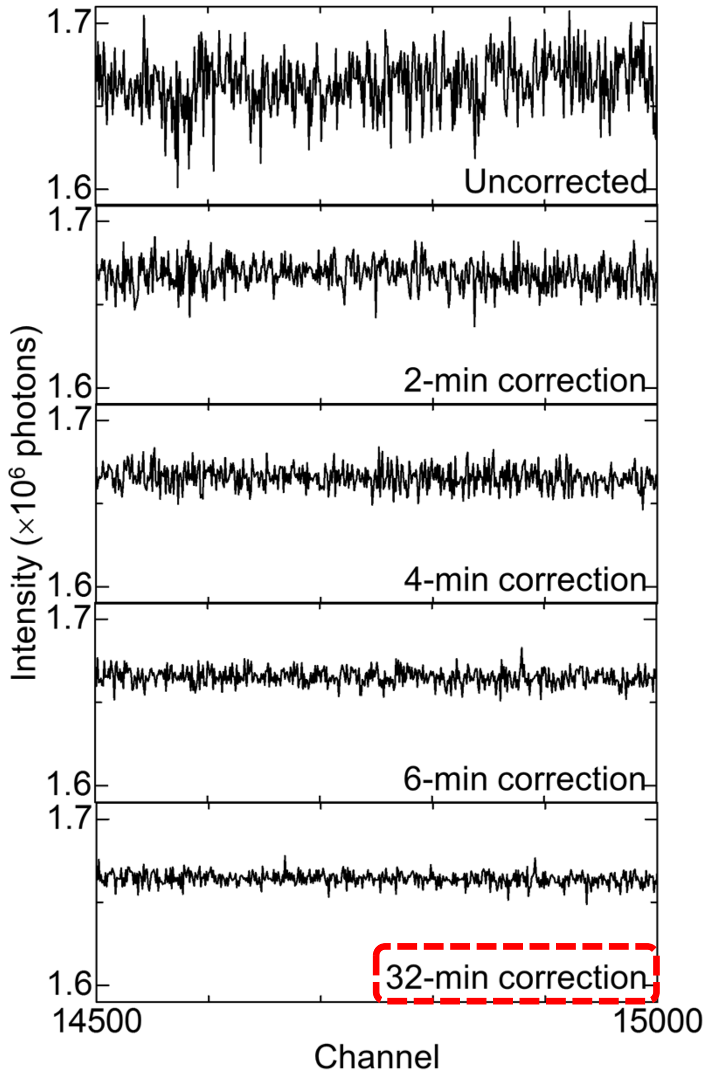


Half a day to half an hour

# Straightforward vs Data-Driven

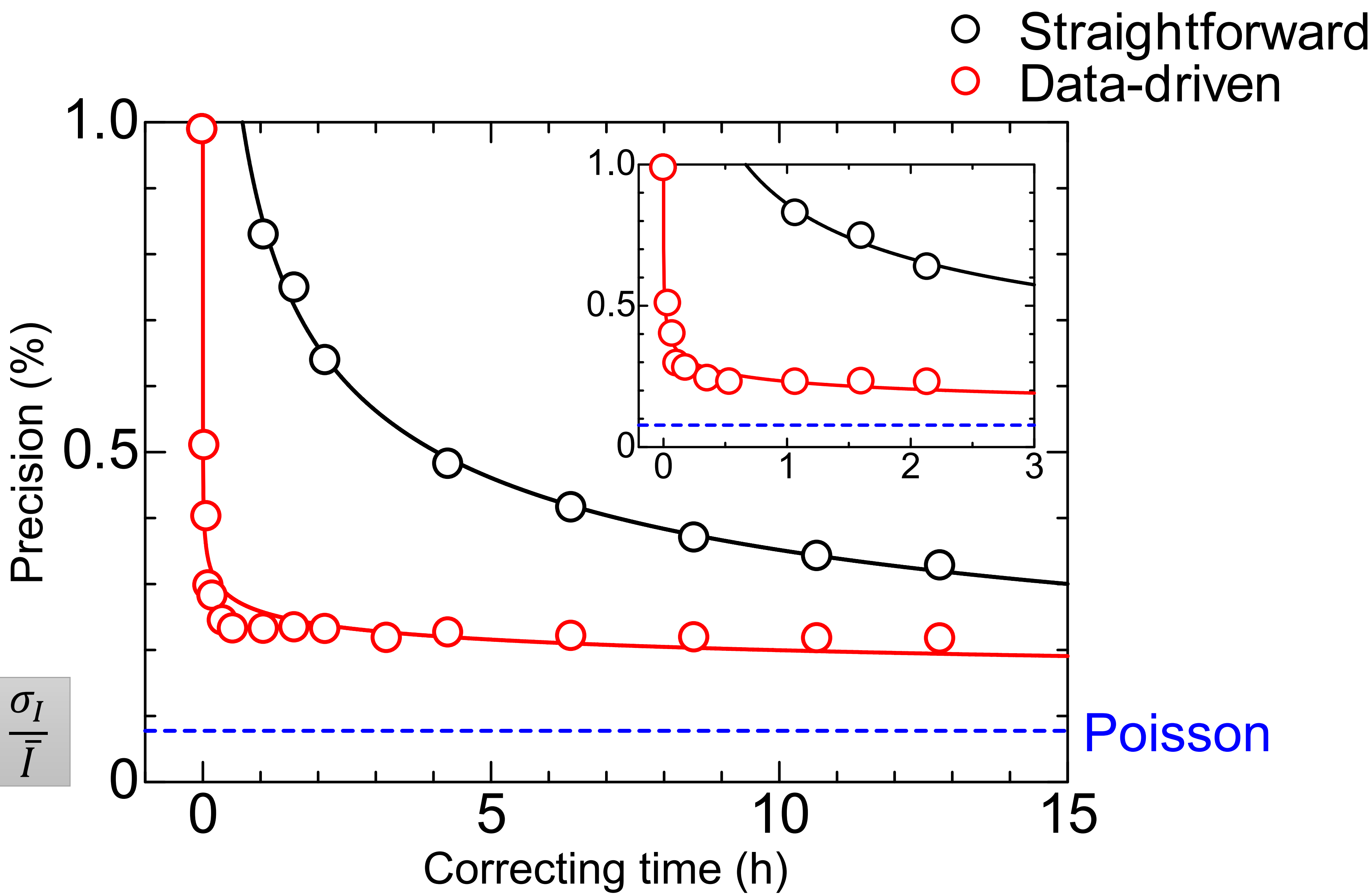


Precision: $\frac{\sigma_I}{\bar{I}}$

# Effects on Diffuse Scattering

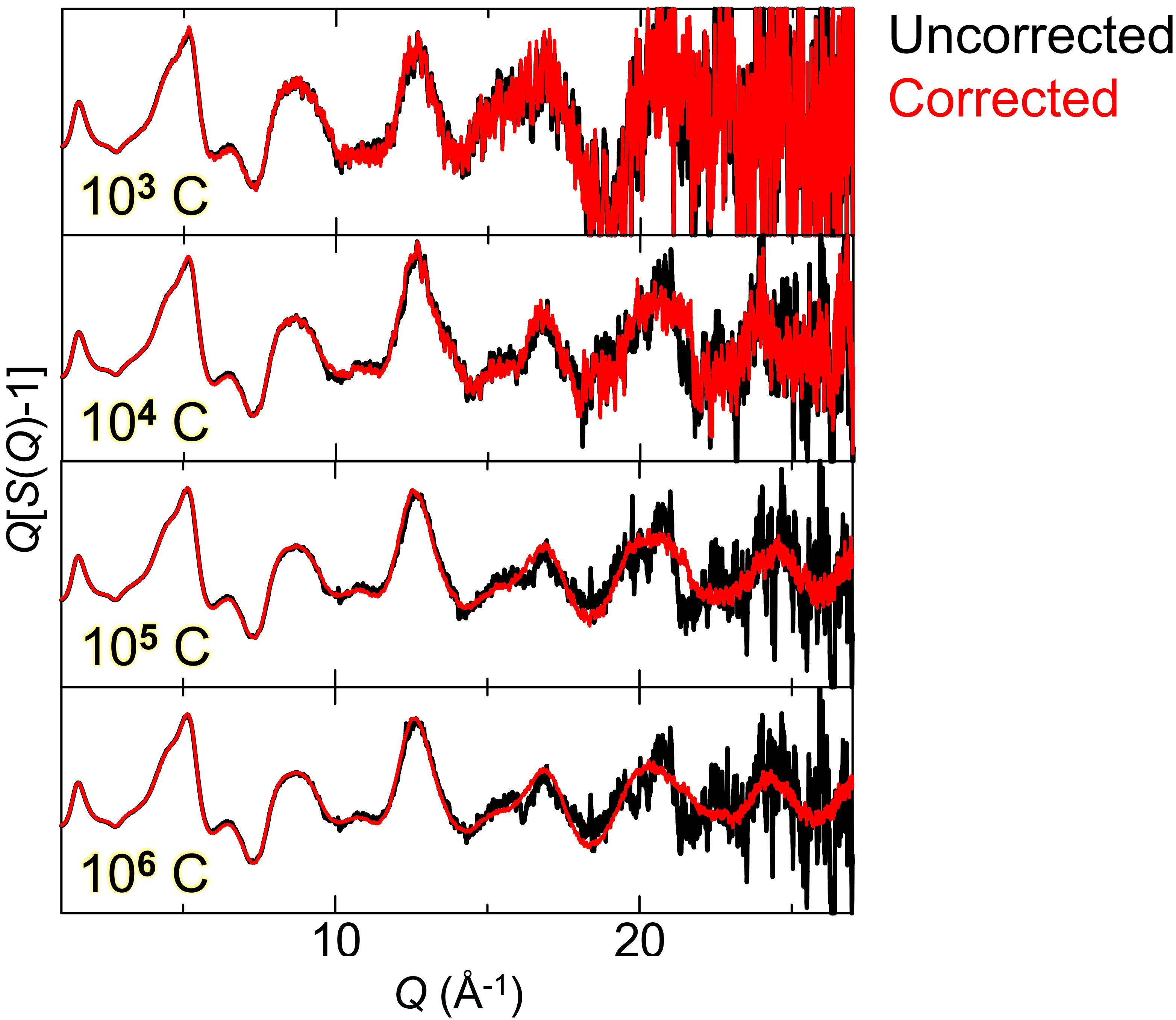

# Effects on Bragg Scattering

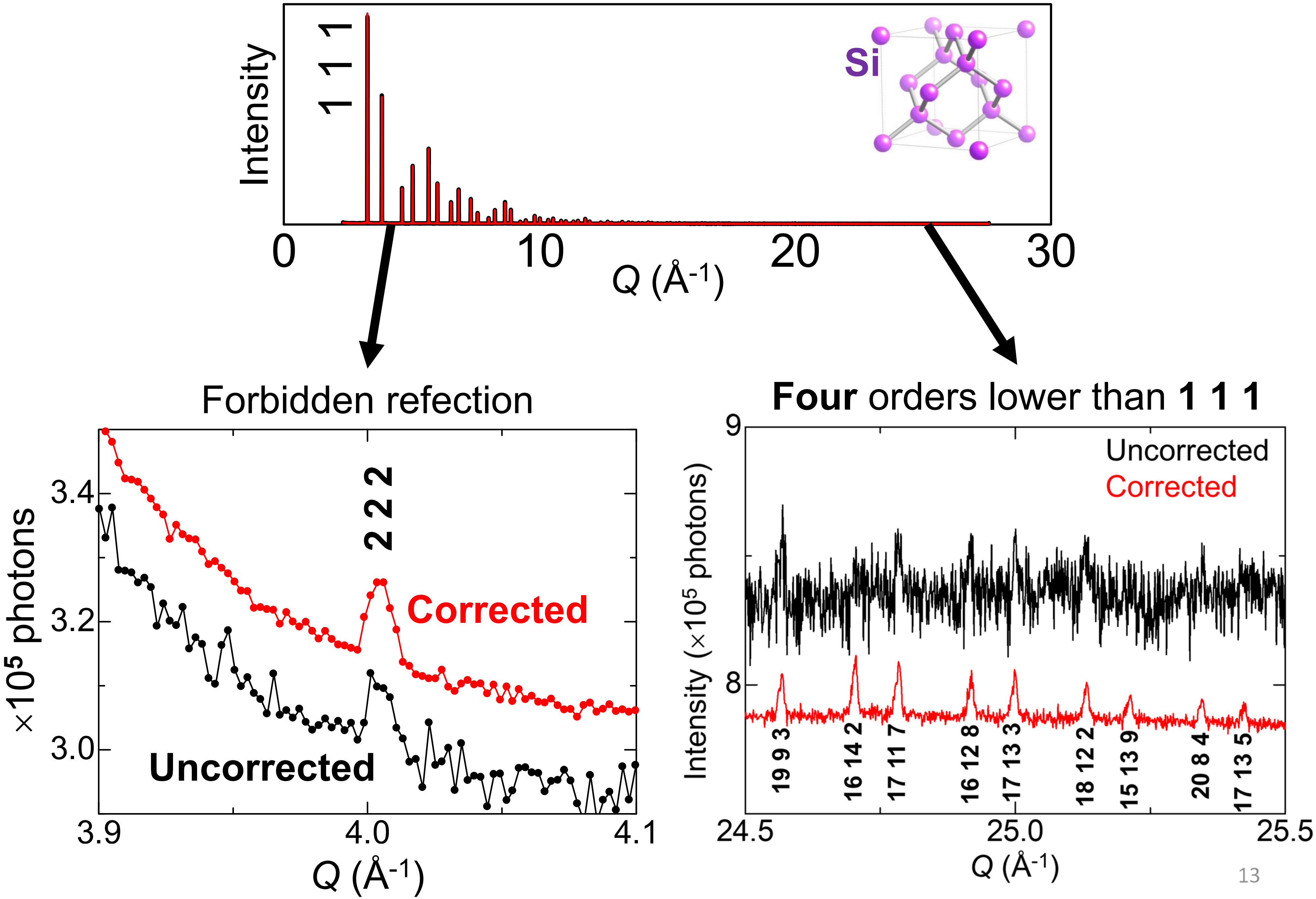

# Restoring Dynamic Range

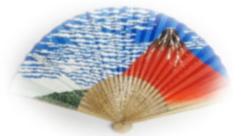

## Hardware: OHGI + Software: ReLiEf

K. Kato et al., *J. Synchrotron Rad.* 26, 762 (**2019**).

K. Kato et al., *J. Synchrotron Rad.* 27, 1172 (**2020**).

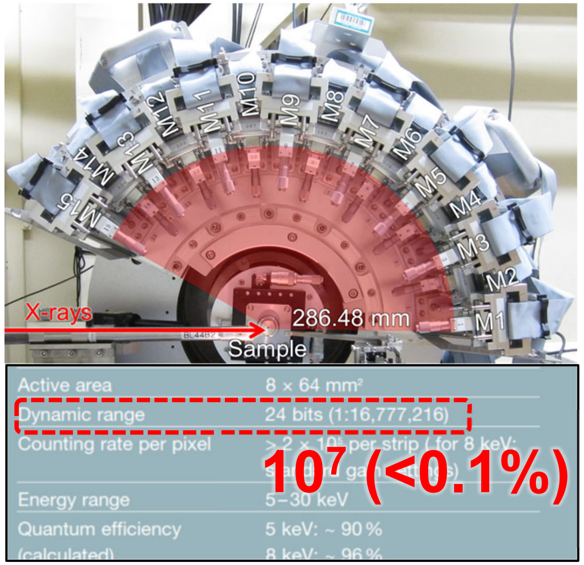


Module spec

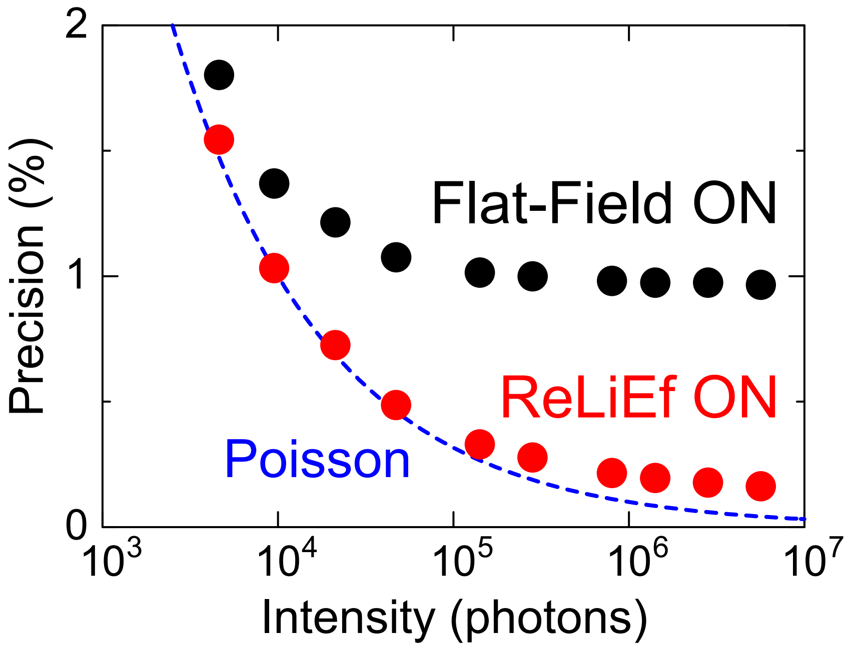


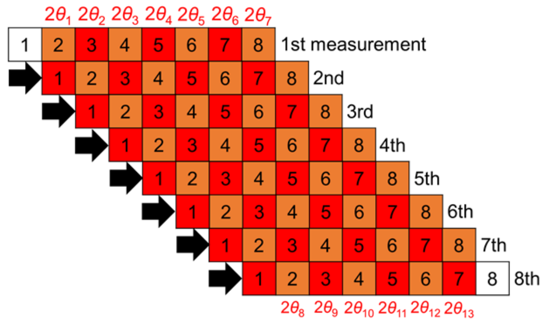


$$c_{\mathrm{OSS}}(1) = \frac{\sum_{k=1}^{7} w_k(1)\, c_{\mathrm{OSS}_k}(1)}{\sum_{k=1}^{7} w_k(1)},$$

$$c_{\mathrm{OSS}}(2) = \frac{\sum_{k=1}^{8} w_k(2)\, c_{\mathrm{OSS}_k}(2)}{\sum_{k=1}^{8} w_k(2)},$$

$$c_{\mathrm{OSS}}(3) = \frac{\sum_{k=2}^{9} w_k(3)\, c_{\mathrm{OSS}_k}(3)}{\sum_{k=2}^{9} w_k(3)},$$

$$c_{\mathrm{OSS}}(4) = \frac{\sum_{k=3}^{10} w_k(4)\, c_{\mathrm{OSS}_k}(4)}{\sum_{k=3}^{10} w_k(4)},$$

$$c_{\mathrm{OSS}}(5) = \frac{\sum_{k=4}^{11} w_k(5)\, c_{\mathrm{OSS}_k}(5)}{\sum_{k=4}^{11} w_k(5)},$$

$$c_{\mathrm{OSS}}(6) = \frac{\sum_{k=5}^{12} w_k(6)\, c_{\mathrm{OSS}_k}(6)}{\sum_{k=5}^{12} w_k(6)},$$

$$c_{\mathrm{OSS}}(7) = \frac{\sum_{k=6}^{13} w_k(7)\, c_{\mathrm{OSS}_k}(7)}{\sum_{k=6}^{13} w_k(7)},$$

$$c_{\mathrm{OSS}}(8) = \frac{\sum_{k=7}^{13} w_k(8)\, c_{\mathrm{OSS}_k}(8)}{\sum_{k=7}^{13} w_k(8)},$$

| | Required | **OHGI+ReLiEf** |
|---|---|---|
| Q range ($Å^{-1}$) | ~30 | ~30 |
| Q step ($Å^{-1}$) | $10^{-3}$ | $10^{-3}$ |
| Precision | 0.1% | 0.1% |

# Precise & Accurate ADPs

K. Kato & B. B. Iversen *et al.*, *IUCrJ* 8, 387 (**2021**).

$$f = f_0 e^{-M}$$

Debye-Waller factor

$$M = 8\pi^2 \langle u^2 \rangle \left(\frac{Q}{4\pi}\right)^2$$

**A**tomic **D**isplacement **P**arameter: *U*

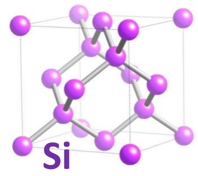


| | Present | References | | | |
|---|---|---|---|---|---|
| | **Total scattering** | **SXRD[1]** | **PND[2]** | **INS[3]** | **CBED[4]** |
| Probe | X-rays | X-rays | Neutrons | Neutrons | Electrons |
| Sample | Powder | Single | Powder | Single | Single |
| $T$ /K | 298 | 293~298 | 284~293 | 293 | 300 |
| $U$ /($10^{-4}$ Å$^2$) | **59.5(1)** | 58.7(1) | 59(3) | 59.4(2) | 58.6 |
| $T$ /K | 100 | -- | -- | -- | 93 |
| $U$ /($10^{-4}$ Å$^2$) | **30.0(1)** | -- | -- | -- | 32.9 |


[1] M. A. Spackman, *Acta Cryst. A* 42, 271 (**1986**).
[2] Z. Baisheng et al., *Acta Cryst. A* 46, 435 (**1990**).
[3] C. Flensburg & F. Stewart, *Phys. Rev. B* 60, 284 (**1999**).
[4] 300 K: Y. Ogata et al., *Acta Cryst. A* 64, 587 (**2008**).
93 K: M. Saunders et al, *Ultramicroscopy* 60, 311 (**1995**).

# Valence Density Studies from Powders

| | |
|---|---|
| Chemical formula | $C_5H_{12}O_5$ |
| Space group | $P2_12_12_1$ |
| $a$ (Å) | 8.2660 (4) |
| $b$ (Å) | 8.8977 (4) |
| $c$ (Å) | 8.9116 (4) |

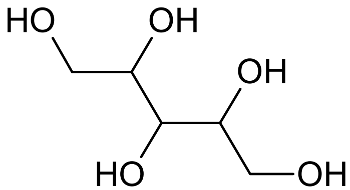


K. Kato & B. B. Iversen *et al.*, *Acta Cryst.* A77, 85 (**2021**).

Static deformation densities 0.1 e $Å^{-3}$ step

Residual densities 0.05 e $Å^{-3}$ step

Powder (Present)

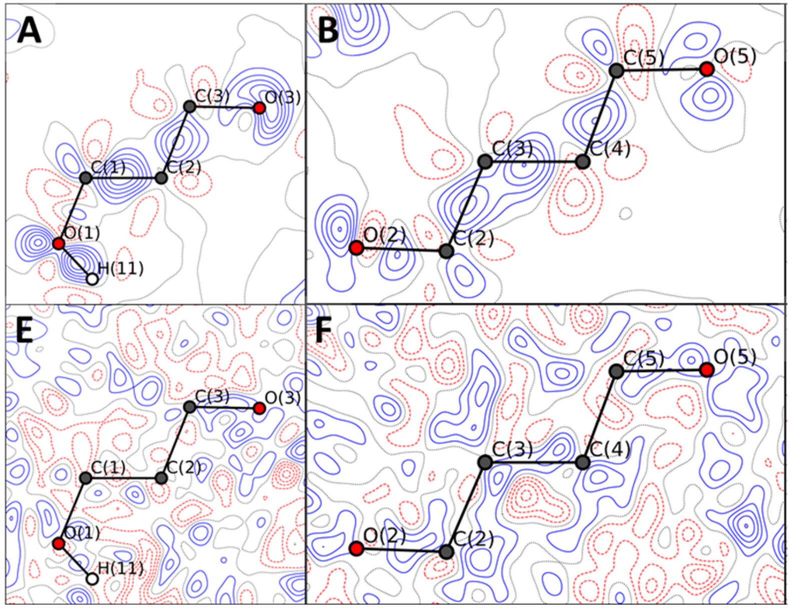


Single crystal (Ref)

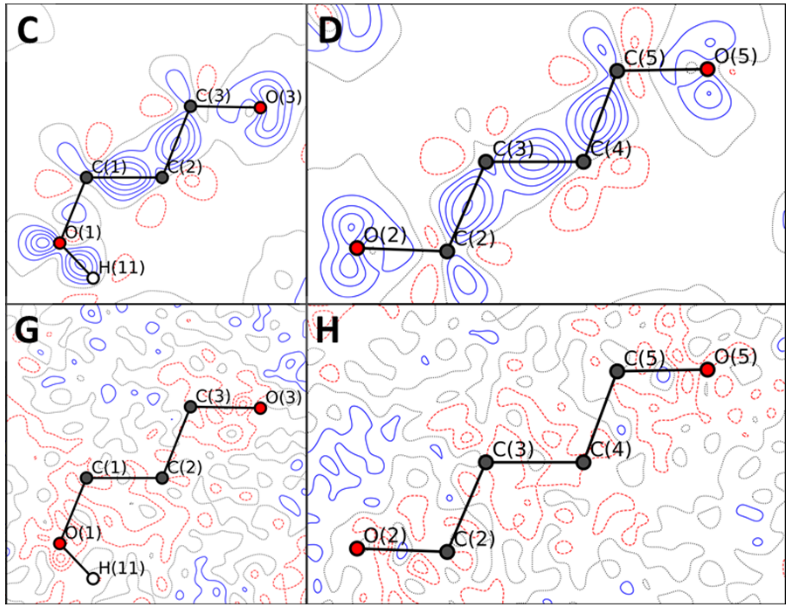


Positive

Negative

A. Ø. Madsen et al., *Acta Cryst. A* 60, 550 (**2004**).

## Comparison in ADPs

| | $\langle U_X^{ii}/U_N^{ii}\rangle$ | $\langle\lvert\Delta U_{X-N}^{ij}\rvert\rangle$ | $\langle\lvert\Delta U_{X-N}^{ii}\rvert\rangle$ | wRMSD |
|---|---|---|---|---|
| **OHGI** | 1.14(5) | 0.0007(5) | 0.0007(5) | 2.14 |
| **Ref.** | 1.21(6) | 0.0012(4) | 0.0011(4) | 3.82 |

Acta Cryst A
FOUNDATIONS
ADVANCES

ISSN 2053-2733

# Nothing trumps good data

**A. Alan Pinkerton***

Department of Chemistry and Biochemistry, University of Toledo, Toledo, OH 43606, USA. *Correspondence e-mail: a.pinkerton@utoledo.edu

Received 21 January 2021
Accepted 21 January 2021

**Keywords:** electron density; data quality; charge density; powder diffraction; MYTHEN detector.

A. A. Pinkerton, "Nothing trumps good data", *Acta Cryst.* A77, 83 (**2021**).

X-rays are scattered by electrons, and the Fourier transform of the X-ray diffraction pattern obtained from a periodic (read crystalline) material is the electron-density distribution in that solid. The details of that distribution depend on the quality of the diffraction data, but even in 1915 it was realized that subatomic details should be available from data of sufficient quality (Debye, 1915). However, it would take decades of hardware and software development to make that a reality.

Although much of the driving force in hardware development could be considered to be reduction in the time required for a diffraction experiment, a frequent consequence was an improvement in data quality. Thus, as the intensity of X-ray beams increased, the ability to detect weaker reflections became possible. As detection of the scattered rays moved from photographic film to point detectors to area detectors, the number of

In this issue, Svane *et al.* (2021) continue the important tradition of evaluating and benchmarking new equipment and techniques, in particular with regard to the use of powder diffraction data to determine the experimental charge density. The microstrip detector (MYTHEN) has a sharper point-spread function than and potentially a similar dynamic range as an image plate (Bergamaschi *et al.*, 2010). However, this dynamic range is significantly reduced by non-uniformity of the X-ray response. Recently, the dynamic range has been largely restored by a statistical approach to the response correction (Kato & Shigeta, 2020). Svane *et al.* (2021) have used the reported image-plate results for diamond as a benchmark to evaluate the data from the MYTHEN detector with the new correction. They used the same Hansen–Coppens/Rietveld strategy as before, and the

with theory (including core polarization), as well as benchmarking a new vacuum image-plate detector (Bindzus *et al.*, 2014).

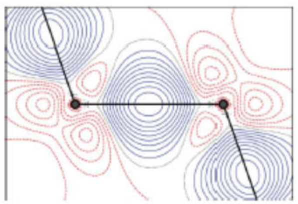

In this issue, Svane *et al.* (2021) continue the important tradition of evaluating and benchmarking new equipment and techniques, in particular with regard to the use of powder diffraction data to determine the experimental charge density. The microstrip detector (MYTHEN) has a sharper point-spread function than and potentially a similar dynamic range as an image plate (Bergamaschi *et al.*, 2010). However, this dynamic range is significantly reduced by non-uniformity of the X-ray response. Recently, the dynamic range has been largely restored by a statistical approach to the response correction (Kato & Shigeta, 2020). Svane *et al.* (2021) have used the reported image-plate results for diamond as a benchmark to evaluate the data from the MYTHEN detector with the new correction. They used the same Hansen–Coppens/Rietveld strategy as before, and the